



ELSEVIER

Available online at www.sciencedirect.com

SCIENCE @ DIRECT®

Physica A 335 (2004) 249–278

PHYSICA A

www.elsevier.com/locate/physa

Generative modelling of regulated dynamical behavior in cultured neuronal networks

Vladislav Volman^a, Itay Baruchi^a, Erez Persi^{a,b},
Eshel Ben-Jacob^{a,c,*}

^a*Raymond and Beverly Sackler Faculty of Exact Sciences, School of Physics and Astronomy, Tel-Aviv University, Tel-Aviv 69978, Israel*

^b*Laboratoire de Neurophysique et Physiologie du System Moteur, Université René Descartes, 75270 Paris, Cedex 06, France*

^c*Kavli Institute for Theoretical Physics, Kohn Hall, University of California at Santa Barbara, Santa Barbara, CA 93106, USA*

Received 3 November 2003

Abstract

The spontaneous activity of cultured in vitro neuronal networks exhibits rich dynamical behavior. Despite the artificial manner of their construction, the networks' activity includes features which seemingly reflect the action of underlying regulating mechanism rather than arbitrary causes and effects. Here, we study the cultured networks dynamical behavior utilizing a generative modelling approach. The idea is to include the minimal required generic mechanisms to capture the non-autonomous features of the behavior, which can be reproduced by computer modelling, and then, to identify the additional features of biotic regulation in the observed behavior which are beyond the scope of the model. Our model neurons are composed of soma described by the two Morris–Lecar dynamical variables (voltage and fraction of open potassium channels), with dynamical synapses described by the Tsodyks–Markram three variables dynamics. The model neuron satisfies our self-consistency test: when fed with data recorded from a real cultured networks, it exhibits dynamical behavior very close to that of the networks' "representative" neuron. Specifically, it shows similar statistical scaling properties (approximated by similar symmetric Lévy distribution with finite mean). A network of such M–L elements spontaneously generates (when weak "structured noise" is added) synchronized bursting events (SBEs) similar to the observed ones. Both the neuronal statistical scaling properties within the bursts and the properties of the SBEs time series show generative (a new discussed concept) agreement with the recorded data. Yet, the model network exhibits different structure of temporal variations and does not recover the observed hierarchical temporal ordering, unless fed with

* Corresponding author. Raymond and Beverly Sackler Faculty of Exact Sciences, School of Physics and Astronomy, Tel-Aviv University, Tel-Aviv 69978, Israel. Tel.: +972-3-640-7845; fax: +972-3-642-2979.

E-mail address: eshel@tamar.tau.ac.il (E. Ben-Jacob).

recorded special neurons (with much higher rates of activity), thus indicating the existence of self-regulation mechanisms. It also implies that the spontaneous activity is not simply noise-induced. Instead, the network seems to possess excitable media like abilities, presumably provided by the underlying glia fabric.

© 2003 Elsevier B.V. All rights reserved.

PACS: 05.70.Ln; 87.17.Aa; 82.40.Bj.

Keywords: Generic modelling; Dynamical systems; Control and regulation

1. Introduction and motivation

Both abiotic and biotic systems can exhibit complex dynamical behavior. Models, together with their analytical and computational studies, have long served as an indispensable tool to discover the principles of dynamical behavior in the physical realm. This approach is consistent with the inherent non-autonomous nature of abiotic systems and the consequent quest for universal underlying principles that govern their behavior. On the other hand, the value and predictive power of models as a research tool in the realm of living systems is still questioned [1,2].

The studies presented here are guided by the proposal that computer modelling can serve as an equally powerful research tool in the studies of biotic systems [3,4]. Provided, though, they are perceived, developed, utilized and analyzed in proper manners adopted to the special autonomous (regulating) nature of these systems. Otherwise, one can easily catch Cowan's "reminiscence syndrome"—the tendency to devise a set of algorithmic rules that mimic some observed features and mistake it for a proper model of the living system, including its underlying autonomous elements which regulate the observed behavior [5]. At the other end there waits the "realistic trap", when the model becomes swamped with so many biological features (included without discrimination), that it loses any predictive power. Following Ref. [1], we emphasize that un-discriminated inclusion of a large collection of biological facts, assembled on the basis of availability, might mask the more essential features and can blur the hidden underlying principles. The way to avoid those pitfalls is the "generative modelling" approach, adopted here. The idea is to elicit, from the observations of several systems belonging to similar class and the knowledge about common general motives in other biotic systems, the generic features to be included in the model. For that, the model is iteratively co-generated with developments of suitable experimental setups, procedures and observables to be measured and utilized for generative cross comparison. The above statements will be discussed for clarification and illustrated via the generative modelling of cultured networks, presented in this paper.

These (in vitro) networks are spontaneously formed from a mixture of cortical neurons and glia cells, homogeneously spread over a lithographically specified area [6–8]. Consequently, the spread cells turned into an active network by sending dendrites and axons, to form synaptic connections for self-wiring. Although the above described

self-wiring process is spontaneous with no externally provided guiding stimulations or chemical cues, a relatively intense dynamical activity is generated within several days. The recorded activity is marked by the formation of synchronized bursting events (SBEs), each being a short (≈ 200 ms) time window during which most of the recorded neurons participate in rapid firing. These SBEs are separated by intervals of sporadic neuronal firing.

The neurons exhibit very rich temporal activity within the SBEs, each with its own time series of spikes (which can vary from burst to burst). Looking at the inter-neuron correlations [9,10] within the SBEs shows that the temporal activity of many neurons is significantly correlated in the temporal pattern of its appearance (the notion “correlated” here is used in the mathematical sense of “similarity”).

To study the statistical scaling properties of the neuronal activity, the time-series is converted into a binary sequence with time bins of 1 ms [6]. For many neurons, the distribution of intervals between firings exhibits a long tail behavior with shorter intervals at the beginning of the SBE and larger ones towards the end. The distribution of the increments of the intervals for these neurons can be approximated with a symmetric Lévy distribution up to the characteristic width of the SBEs (for concise description of Lévy distributions, see the appendix or Refs. [11–14]). More details are presented in the next section.

Segev et al. [6] proposed that the time-series of the SBEs can be utilized as an additional important quantifiable observable to describe the network activity when regarded as one unit. For that, it is convenient to construct a binary sequence representation for the SBEs time-series, using the time width of the SBEs as the basic time bin (typically 100–200 ms vs. the 1 ms for the individual neurons activity). Illuminating example of such binary sequence, together with the corresponding distributions of its intervals (the inter-SBEs intervals) and the interval increments are also shown in the next section. As is illustrated, the interval distributions have a cutoff interval, $I_{\min} \approx 1$ s, and a most probable interval $I_{mp} \approx 5$ s. The distributions are not symmetric about the latter with an average interval $I_{av} \approx 10$ –20 s and a scale-free (algebraic) tail. The increments distributions are symmetric about zero (equal positive and negative distributions) and can be approximated by a zero-mean symmetric Lévy distributions [6]. Interestingly, I_{mp} and I_{av} of very different cultured networks (from 50 to 10^6 neurons) have very similar values, thus hinting about self-regulation of the spontaneous activity. Additional hints are provided by the observations of long time correlations in the SBEs temporal ordering, and in some networks also hierarchical temporal organization (i.e burst of SBEs, bursts of bursts of SBEs up to four detectable hierarchical levels). The spontaneous activity of some networks can also be partitioned into subgroups of different kinds of SBEs yet with a mixed temporal ordering of appearance [9,10]. Put together, the above observations hint that the spontaneous activity of cultured networks might be self-regulated despite the artificial nature of their construction. Much attention has been devoted to the excitable media behavior of glial network and to the neuro-glia interaction [15]. Motivated by the new findings, Hulata et al. [16] and Baruchi and Ben-Jacob [10] proposed that the cultured networks activity is cooperatively regulated by the neurons and the glia, so that the networks should be viewed as a neuro-glia fabric rather than stand alone neuronal networks.

From modelling perspective, it has been shown that a network composed of Integrate-and-Fire elements connected via dynamic synapses can produce SBEs [7,17]. Yet, the internal neuronal activities of such simulated bursts qualitatively differ from the observed ones. Also, the simulated SBEs time series does not show the observed heavy-tailed Lévy-like statistics. Thus, our first goal was to identify the additional minimal generic features required for: (1) generation of temporally localized SBEs, together with internal long-tailed neuronal activity; (2) generation of a sequence of relatively similar SBEs (similar time width and internal neuronal activity), together with long-tailed distributions of intervals between the SBEs and Lévy-like statistics of the sequence increments.

From dynamical systems perspective, an integrate-and-fire (IF) element has one variable (the voltage) dynamics with externally imposed singularity: generation of a voltage spike and setting the voltage to zero when it reaches a threshold. On the other hand, to capture the features of synaptic plasticity (self-regulation), the synapses are now commonly described as a dynamical system with two or more state variables with corresponding coupled ODEs [17]. Thus, to maintain proper matching in the level of description of the neuron soma (the neuron cell body) dynamics with that of its synapses, one may represent the soma as a two-variables dynamical system.

The original detailed Hodgkin–Huxley [18,19] neuronal model is equivalent to a four-variable dynamical system. Such detailed description is required if one is interested in the voltage–current temporal profile (temporal structure) of neuronal action potential. Namely, on time scales of about and below 1 ms. Qualitatively bridging between the dynamical systems perspective and the soma “physiology”, the levels of description are [19]: (1) the soma voltage, which is increased by the input signals and decreased by leaking membrane currents between events of firing (generation of action potentials); (2) the opening and closing of potassium (K^+) channels between and during neuronal firing; (3) the opening and closing of sodium channels (Na^+). These channels have shorter time scales relative to the potassium ones; (4) inclusion of additional channel states, e.g. instead of open and closed also active (channels that can open) and inactive ones with appropriate dynamical transitions in between; (5) slow alterations of membrane properties, such as expression of new channel proteins and receptors and changes in local receptor density.

The rationale for the common use of the IF elements in models of neural networks stems from the view that on the time scales of network activity the dynamical equation for the voltage should be sufficient, as it represents the “proper” time scales of interest, which are longer than 1ms when the network dynamics is considered. However, including only the voltage dynamics means that only local (in time) information affects the soma, since all soma memory effects described by the channel dynamics are neglected. This is not consistent with the fact that, during the real network activity, the inputs received by the neuron from other neurons have special temporal ordering. So that for such temporally ordered inputs to be meaningful, the soma must utilize memory means. Following this simple reasoning, we assumed that memory features should be added to the dynamical description of the soma.

Guided by the above realization, we looked for a model in which the soma is described by at least two degrees of freedom. The two natural candidates are the

FitzHugh–Nagumo model [20,21] and the Morris–Lecar model [22]. For the additional reasons, we have adopted the Morris–Lecar (M–L) dynamical description: (1) in the M–L element, memory can be related to the dynamics of potassium channels; (2) it has been shown by Abbott and Kepler [23] that the M–L equations can be viewed as a reduction (to two variables) of the Hodgkin–Huxley model; (3) the M–L dynamical system has a special phase-space, which can lead to generation of scale-free behavior when fed with a simple noise current (Section 3).

To further check the validity of the M–L element, when combined with dynamical synapses, in representing the observed neuronal activity, we have imposed the following self-consistency requirement: the modelled neuron should exhibit similar activity to that of the recorded ones when it is fed with recorded neuronal activity through Tsodyks–Markram modelled dynamical synapses (Section 3). We reflect on the issue of comparison between the modelled neuron and the real ones. Specifically, we elaborate on the generative comparison approach and demonstrate that it can be utilized to identify new features associated with neuronal self-organization although these features are not included in the model.

Additional discussion of the generative comparison idea is presented in Section 4, in which we study a network of M–L elements connected by the dynamical synapses [17]. Utilizing the modelled network we could generate SBEs with similar statistical properties (Lévy-like distribution in the increments) as the observed ones. We also show that the average synaptic strength affects the internal temporal structure of the SBEs but has little effect (within limits) on the statistical properties of their time series. Both the inter and intra temporal properties of the SBEs can be modified if the functional distribution of the synaptic strengths is changed. These results provide important clues about possible networks' self-regulation. We also studied the effect of the statistical properties of external input currents (in addition to the internal cross-neuronal ones) on the networks' activity. For example, we show that time correlations in the external current have strong effect on the long tail behavior of the SBEs time series.

In the last section, we reflect on the possible implications of these and additional findings about self-regulation motives in cultured networks, with emphasis on a possible new schema of neuro-glial cooperative dynamical behavior. In this schema, the recorded neuronal activity is assumed to be a “pattern on top of pattern”, with the underlying pattern being associated with the web of glia cells.

2. The observed generic features

The spontaneous activity of cultured networks is recorded by growing dissociated cultures of cortical neurons and glia cells on top of multi-electrode array (MEA) composed of 60 electrodes. Neurons drawn from 1-day-old *Charles Rivers* rats are prepared and maintained according to the protocol described in Ref. [6]. Consequently, the spread cells turn into a network by sending dendrites and axons, to form synaptic connections for self-wiring [7,9,24]. Although the above described self-wiring process is spontaneous with no externally provided guiding stimulation or chemical cues, a

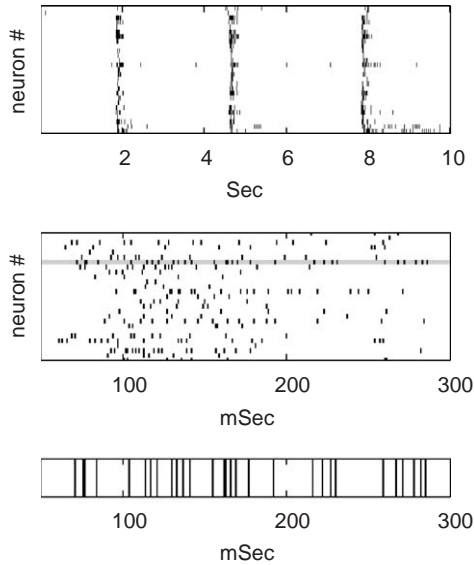


Fig. 1. An example of a raster plot presentation of the recorded network activity showing the SBEs (top panel), and a closer look at an individual event (middle panel). An SBE is detected whenever the number of neurons that fired during a time segment of 100 ms exceeds a threshold (usually taken to be 80% of the total number of recorded neurons). The binary representation of single neurons' activity is shown on the bottom panel, to illustrate the unique pattern of each neuron.

relatively intense activity is self-generated within several days. The networks activity is non-invasively recorded as several (tens) of the neurons form capacitive coupling with the electrodes, thus enabling the recording of their action potentials. A raster plot of a typical activity of a normally developed network after 10 days in culture is presented in Fig. 1. The predominant feature of the activity is the formation of SBEs, each being a short ~ 100 – 200 ms time window during which most of the recorded neurons fire several times at a relatively high rates. The SBEs are separated by long (above seconds) intervals of sporadic neuronal firing. Long term recording shows that this kind of spontaneous activity can continue for several weeks, keeping a steady (averaged) rate of SBEs formation.

2.1. Generic features of the intra-SBEs neuronal activity

During the SBEs each neuron has its own temporal pattern of firing (time-series of spikes), as presented in Fig. 1. Both the firing rate and the time-series statistical properties can greatly vary from neuron to neuron. While some neurons fire only 1–2 spikes/SBE, others can fire even 30 spikes/burst. The individual neuron activity can also vary from SBE to SBE. In Fig. 2, we illustrate the variations in the neuronal activity, both between different SBEs and between different neurons. Despite the large variations, the combined (over different SBEs) histogram of inter-spike intervals of many neurons

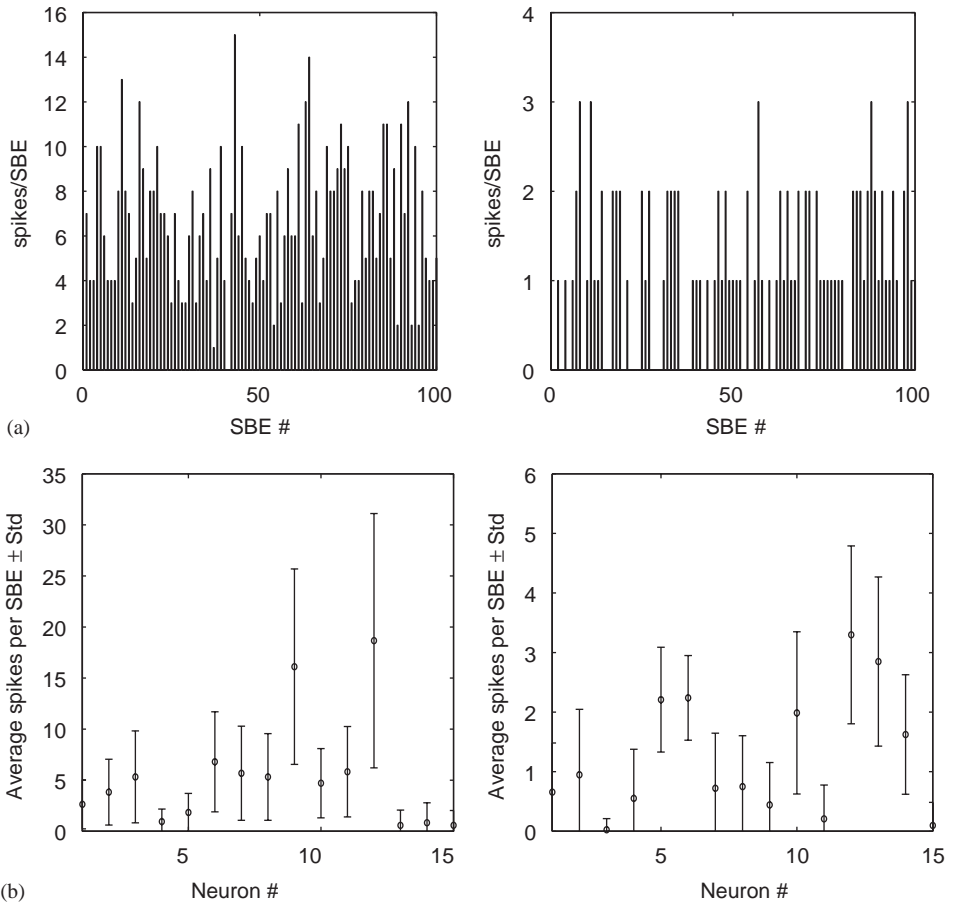


Fig. 2. Illustration of the variation in the rate of neuronal firing. (a) Two examples of variations of individual neuron firing between different SBEs: left: for the network shown in Fig. 1; right: for a different network which exhibits slower neuronal firing. (b) The corresponding variations between neurons for the two networks.

has similar statistical features, and the distribution of the increments of the inter-spike intervals (denoted $\delta(i)$ following Ref. [7]) can be approximated by a symmetric Lévy distribution (the appendix). In Fig. 3a, we show the averaged (combined over all the neurons) distribution of the increments. For comparison, we also show in Fig. 3b the distribution of a “representative”, or a “typical” neuron, constructed as follows: first, several neurons whose rate of activity is close to the typical rate and the variation in their activity between SBEs is close to the typical one are selected. Second, their combined distribution is evaluated as if they represent an individual neuron recorded over corresponding number of SBEs. We emphasize that the above described procedure is oversimplified and aimed just to illustrate the proposed notion of representative

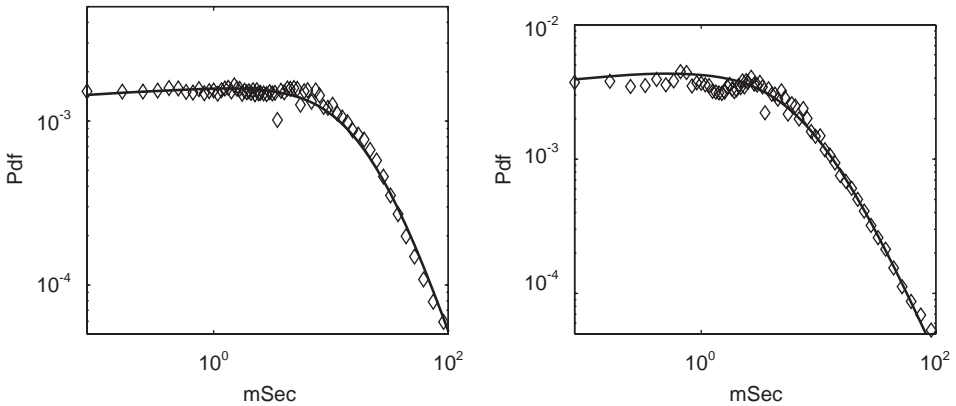


Fig. 3. Left: The combined (averaged) distribution of the increments. That is, the distribution includes the measured increments for all the neurons. The solid line is a symmetric Lévy distribution with $\alpha = 1.05$ and $\gamma = 20$. Right: The increments distribution for a “typical” neuron, constructed as explained in the text. The solid line is a symmetric Lévy distribution with $\alpha = 0.9$ and $\gamma = 9$.

neuron, vs. “averaged” distribution. In many cases (e.g. when the activity is partitioned into significant sub-groups of SBEs and of neurons), several representative neurons have to be constructed, each to describe a distinct observed sub-group. Moreover, there is no “optimal prescription” how to construct the “representative neuron” as its meaning varies according to the special features of interest.

2.2. Generic features of the SBEs binary sequence

To analyze the statistical scaling properties of the SBEs time series it is convenient first to convert the recorded activity into a binary sequence: the time axis is binned according to the typical SBE time width, and the “1”s of the sequence mark the events’ locations. An illuminating example of such binary sequence together with the corresponding distributions of its intervals (the inter-SBEs intervals) and the intervals increments are shown in Fig. 4. As we have mentioned in the introduction, the intervals distributions have a cutoff interval $I_{\min} \sim 1$ s and a most probable interval $I_{mp} \sim 5$ s. The distributions are not symmetric about the latter with an average interval $I_{av} \sim 10\text{--}20$ s and long tail behavior. The increments distributions are symmetric about zero (equal positive and negative distributions) and can be approximated by symmetric Lévy distributions [7]. Segev et al. found that the Lévy-like scaling statistics is common to cultured networks ranging from 50 neurons spread over $1\text{ mm} \times 50\text{ }\mu\text{m}$ area, to $O(10^6)$ neurons spread over 2 cm^2 area. All these networks also exhibit similar long time correlation and similar values of the most probable intervals between SBEs, despite the large size differences between them. The above, together with the additional features described in the Introduction, led us to assume that the spontaneous activity of cultured networks is not completely arbitrary (non-autonomous), but also expresses self-regulation (autonomous) motives.

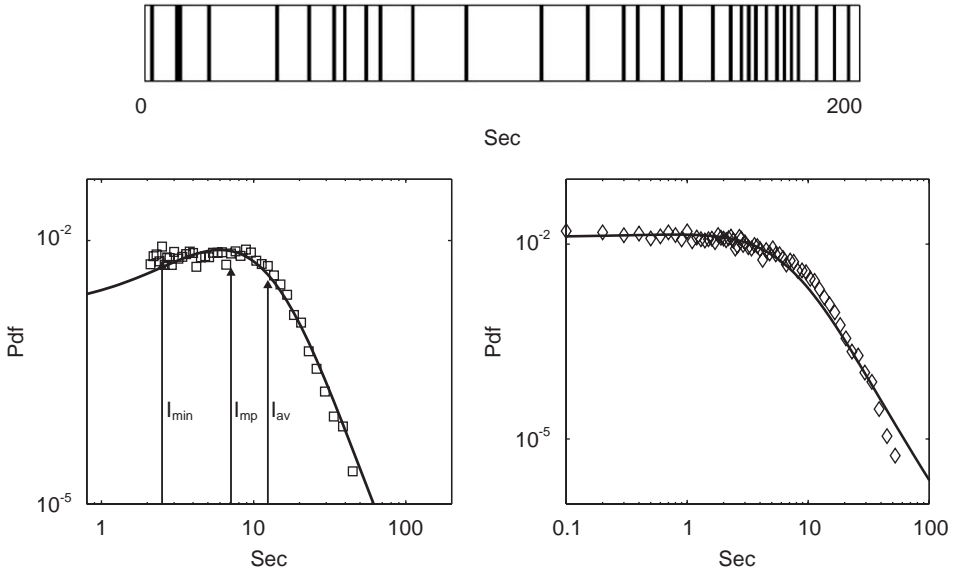


Fig. 4. Top: A binary sequence representation of networks' activity, constructed as explained in text. Bottom left: the distribution of the inter-SBEs intervals. The vertical lines, I_{min} , I_{mp} , I_{av} are the minimal, most probable and average intervals, respectively. The solid line is a symmetric Lévy distribution with $\alpha = 1.8$, $\gamma = 35$ and $\delta = 100$. Bottom right: the pdf (probability density function) of the increments of the intervals on a double logarithmic scale. The solid line is a symmetric Lévy distribution with $\alpha = 1.7$ and $\gamma = 45$.

3. The generic neuron model

In this chapter, we present the minimal generic features required to capture the long tail distributions of the neuronal firing sequences within the SBEs. These included features are: (1) Neuronal dynamical threshold—each neuron is a dynamical system described by two variables. One corresponds to the membrane voltage and the second determines the threshold voltage for generation of action potential [25]. (2) Dynamic synapses—each synapse is described as a three variables dynamical system to model the pre-synaptic kinetics associated with neuro-transmitters. These variables correspond to the relative fractions of neuro-transmitters in the inactive, recovered and active states. The model is tested utilizing the model neuron as is described in Section 3.3, by driving through modelled synapses signals recorded from a real cultured network.

3.1. Two variables dynamic neurons

For reasons presented in the introduction, we have selected to describe the neuronal dynamics utilizing the M–L model [22]. A simple version of this model can be

represented by the following two coupled non-linear equations [22,19,26]:

$$\dot{V} = -I_{ion}(V, W) + I_{ext}(t), \quad (1)$$

$$W(\dot{V}) = \phi \frac{W_{\infty}(V) - W(V)}{\tau_W(V)}, \quad (2)$$

where $I_{ion}(V, W)$ represents the contribution of the internal ionic Ca^{2+} , K^+ and leakage currents with their corresponding channel conductivities g_{Ca} , g_{K} and g_L being constant. Namely

$$I_{ion}(V, W) = g_{\text{Ca}}m_{\infty}(V)(V - V_{\text{Ca}}) + g_{\text{K}}W(V)(V - V_{\text{K}}) + g_L(V - V_L). \quad (3)$$

On the other hand, I_{ext} represents all the external current sources stimulating the neuron, such as signals received through its synapses, artificial stimulations as well as any noise sources.

$W(V)$ in Eq. (2) represents the fraction of open potassium (K^+) channels. In the absence of stimulations, $W(V)$ relaxes towards its limit value (nullcline) $W_{\infty}(V)$, which is assumed to have the following sigmoid shape:

$$W_{\infty}(V) = \frac{1}{2} \left(1 + \tanh \left(\frac{V - V_1}{V_2} \right) \right) \quad (4)$$

within a characteristic time scale given by

$$\tau_W(V) = \frac{1}{\cosh((V - V_1)/2V_2)}. \quad (5)$$

In principle, one should write a similar dynamical equation to describe the fraction of open Ca^{2+} channels. Inclusion of such equation is important when one is interested in the profile of the action potential. Here we focus on the statistical scaling properties of the neuronal firing time series. Therefore, only the temporal location of neuronal firings is relevant, so we can represent the effect of the Ca^{2+} channels by the limiting sigmoid $m_{\infty}(V)$ (the parallel of $W_{\infty}(V)$), which is given by

$$m_{\infty}(V) = \frac{1}{2} \left(1 + \tanh \left(\frac{V - V_3}{V_4} \right) \right). \quad (6)$$

In our numerical simulations, we have used the following values: $g_{\text{Ca}}=1.1 \text{ mS/cm}^2$, $g_{\text{K}}=2.0 \text{ mS/cm}^2$, $g_L=0.5 \text{ mS/cm}^2$, $V_{\text{Ca}}=100 \text{ mV}$, $V_{\text{K}}=-70 \text{ mV}$, $V_L=-34.32 \text{ mV}$, $V_1=-1 \text{ mV}$, $V_2=15 \text{ mV}$, $V_3=10 \text{ mV}$, $V_4=14.5 \text{ mV}$, $\phi=0.3$. With such a choice of parameters, $I_c=0$.

Application of the phase-space analysis to the M–L system reveals the existence of several regimes [22,26]. Of special interest to us is the situation in which oscillations with controlled low frequency emerge as the system undergoes saddle-on-node bifurcation. In this case, a DC external current plays the role of a bifurcation parameter (Fig. 5). In the excitable phase, the system spends most of the time at the stable fixed point. Short excursions in the outer part of the phase space are possible only if noise is added. The threshold is well-defined, and scales as the distance between stable and saddle fixed points. When the value of bifurcation parameter is further increased, the

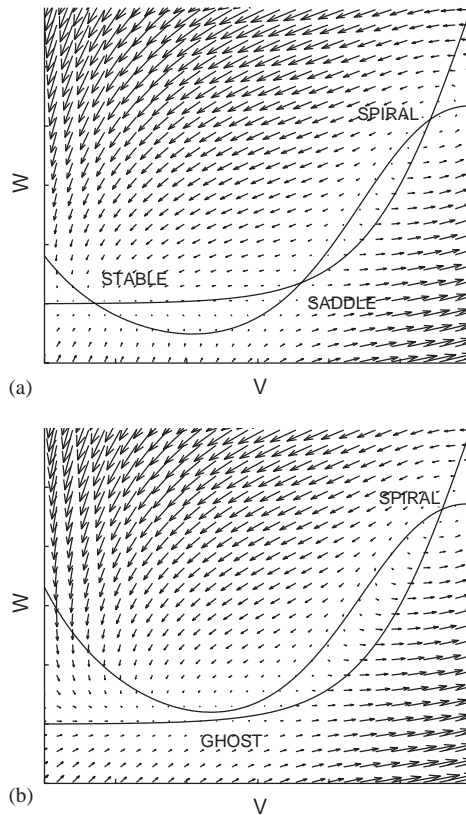


Fig. 5. Phase space, illustrating dynamics of M–L element. Each arrow is a vector \mathbf{r} , defined by the pair of variables: $\mathbf{r} \equiv (\dot{V}, \dot{W})$. Below the critical current I_c (in the excitable phase), there is a stable (attractive) fixed point. Hence, neuronal firing is possible only due to noise (a). Above I_c (b), the dynamics is composed of a series of neuronal spikes. The inter-spike intervals scale as explained in text.

two fixed points approach each other and finally coalesce, leading to the emergence of a stable limit cycle oscillations with controlled low frequency. Such flat coalescence of a stable and a saddle fixed points offers generic recipe allowing the emergence of scale-free statistics. This possibility arises as a result of the scaling relation between period of oscillations and the external current, given by

$$\langle ISI \rangle \propto (\langle I \rangle - I_c)^{-0.5}, \tag{7}$$

where ISI is the inter-spikes interval, I is the stimulating current and I_c is a critical current. Consequently, time-dependent current added to a DC current close to I_c can lead to a very rich neuronal dynamics.

As the value of the DC current is further increased, there is a second phase transition. When $W_\infty(V)$ crosses the maximum of V -nullcline, the focus turns to be an attractor. At current levels above this second critical value, the neuron behaves like a decaying

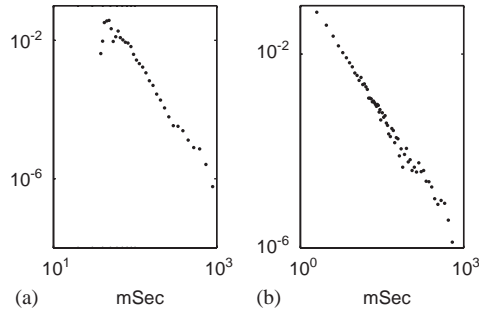


Fig. 6. Temporal activity of a noise-driven neuron: (a) Inter-spike interval distribution. The distribution extends over several time decades, indicating possible temporal scaling; (b) pdf of $\delta(i)$. The distribution is heavy-tailed and linear on the log–log scale.

oscillator. Thus, we expect that the M–L description of spiking will be valid only for oscillations with a period larger than the certain cutoff period. The origin of this cutoff lies in the finite membrane response time. To obtain a correct description of the activity on even shorter time scales, additional features have to be included.

Keeping in mind modelling of spontaneous activity of isolated cultured network, we set to test the response of the model neuron to external noise currents. This issue becomes particularly important in light of the recent findings that this class of models exhibits high noise sensitivity [27–29]. We found that it is possible to generate a scale-free distribution of intervals by stimulating a modelled neuron with random walk currents. We impose reflecting boundary conditions on the random walk, to limit the noise amplitude. Specifically, we require that $0 \mu\text{A}/\text{cm}^2 \leq I_{\text{noise}} \leq 0.86 \mu\text{A}/\text{cm}^2$. Hence, a neuron is restricted to the limit-cycle phase. Every time step (of 0.1 ms each), a value of I_{noise} is either incremented or decreased, with equal probability, by a value of $|\Delta I_{\text{noise}}| = 0.1 \text{ nA}/\text{cm}^2$. In Fig. 6, we demonstrate long tail behavior both in the distribution of the intervals between neuronal firing and in the increments of the intervals. For a neuron stimulated by single noisy link, we have seen how certain noise characteristics lead to the emergence of heavy-tailed distribution. In order for neuron to retain this feature in the *network*, where it is stimulated by many links, certain constraints have to be imposed on the couplings between neurons. Coupling strength must not be too strong, so that it will not completely suppress the individuality of neurons. On the other hand, an extremely weak coupling will not have any significant influence. Thus, the optimal coupling mechanism must introduce only a *tendency* to synchronization in activity of different neurons. This requirement is satisfied by the synaptic dynamics, as we explain next.

3.2. Dynamic synapses

Different means of synaptic plasticity are classified according to the time scale on which they are expressed: short-term (seconds and minutes) and a long-term (hours, days and months). Quantal analysis demonstrates that short-term modifications in

synaptic strength are due to a pre-synaptic changes in the number of quanta of transmitter released by incoming impulses. For example, depression may be explained as being due to a limited stored amount of releasable transmitter, which can be depleted by a train of arriving stimuli and not given sufficient time for replenishment [19,30]. Likewise, short-term potentiation and facilitation are conveniently described using the pre-synaptic state parameters. In general, short-term synaptic plasticity is associated with changes in the state of the pre-synaptic site only. On the other hand, long-lasting forms of plasticity usually require some involvement from the post-synaptic side as well. For example, long-term potentiation is initiated when the pre- and post- synaptic neurons are correlated.

In the model of short-term synaptic dynamics put forth by Tsodyks et al. [17], the effective synaptic strength evolves according to the following equations:

$$\dot{x} = \frac{z}{\tau_{rec}} - ux\delta(t - t_{sp}), \tag{8}$$

$$\dot{y} = -\frac{y}{\tau_{in}} + ux\delta(t - t_{sp}), \tag{9}$$

$$\dot{z} = \frac{y}{\tau_{in}} - \frac{z}{\tau_{rec}}. \tag{10}$$

Here, x , y , and z are the fractions of synaptic resources in the recovered, active and inactive states, respectively. The time-series t_{sp} denote the arrival times of pre-synaptic spikes, τ_{in} is the characteristic time of post-synaptic currents (PSCs) decay, and τ_{rec} is the recovery time from synaptic depression. Obviously, the resource conservation law holds for all times:

$$x + y + z \equiv 1. \tag{11}$$

The variable u describes the effective use of synaptic resources by the incoming spike. For facilitating synapses, it obeys the following dynamic equation:

$$\dot{u} = -\frac{u}{\tau_{facil}} + U_0(1 - u)\delta(t - t_{sp}), \tag{12}$$

where the parameter U_0 determines the increase in the value of u with each spike. If no spikes arrive, the facilitation parameter decays to its baseline value with the time constant τ_{facil} . For the depressing synapses (as is the case when post-synaptic neuron is excitatory) one has $\tau_{facil} \rightarrow 0$, and $u \rightarrow U_0$ for each spike.

The effective synaptic current of a neuron i is obtained by summing all of its j synaptic currents:

$$I_{syn}^i = \sum_{j \neq i} A_j y_j(t). \tag{13}$$

For the time being, we assume that the parameters A_j , which represent contribution of the post-synaptic side to the synaptic strength, do not change with time. In reality, however, we know that long-lasting forms of plasticity require some involvement from the post-synaptic side [31,19]. Thus, the model that was described above is supposed to

account for up to hours plasticity, but not for the long-term one. The effects of synaptic scaling are included in a similar model using different description for the two variable behavior of the model neuron [25]. It is shown that when self regulated long-term modulations of synaptic strengths are included, they lead to similar generic results as we report here.

The values of parameters control the ability of system to exhibit modes of correlated activity. In our studies (unless indicated otherwise), we assigned to the network the average parameters specified below, using the following notations: I indicates inhibitory neurons and E —excitatory ones. For example, $\tau_{rec}(E \rightarrow I)$ refers to the recovery time of a synapse transmitting input to an inhibitory neuron from excitatory one. Hence, we set: $\tau_{rec}(I \rightarrow I) = 200$ ms, $\tau_{rec}(E \rightarrow I) = 200$ ms, $\tau_{rec}(I \rightarrow E) = 1200$ ms, $\tau_{rec}(E \rightarrow E) = 1200$ ms, $U_0(I \rightarrow I) = 0.5$, $U_0(E \rightarrow I) = 0.5$, $U_0(I \rightarrow E) = 0.08$, $U_0(E \rightarrow E) = 0.08$, $A(I \rightarrow I) = 9$, $A(E \rightarrow I) = 9$, $A(E \rightarrow E) = 2.2$, $A(I \rightarrow E) = 6.6$. Actual values for each neuron were then generated as reported in Ref. [17]. We set $\tau_{in} = 6$ ms for all neurons. In addition, due to the small size of our simulated network, we chose $\tau_{facil} = 2000$ ms for all inhibitory neurons.

3.3. A self-consistency test: Feeding the neuron with recorded data

In the previous section, we demonstrated that the M–L dynamics can generate scale-free behavior when driven by a simple (bounded) random walk currents. The additional requirement is the ability of many linked M–L elements to generate the observed SBE. In order to test the existence (in principle) of such dynamical behavior in a network of M–L elements, we drive a single element with recorded data drawn from the spontaneous activity of a cultured network. For N simultaneously recorded neurons, we first selected randomly 80% to play the role of excitatory and 20%—inhibitory ones. The synaptic constant strengths (A_{ij}) are normally distributed about an average value A_0 . In addition, a noise current $I_{noise}(t)$ is included. So the combined external current, as “seen” by a model neuron, is

$$I_{ext}(t) = \sum_{j=1}^N A_j y_j(t) + I_{noise}(t), \quad (14)$$

where $y_j(t)$ obey the modelled synaptic dynamics. A typical example of such self-consistency test is shown in Figs. 7 and 8. As expected, the model neuron generates rapid firing activity during SBEs in the recorded data. Moreover, within the SBEs the time series of the modelled neuron activity exhibits a scaling behavior, whose increments can be approximated with a symmetric Lévy distribution. Using the maximum-likelihood method, the scaling behavior corresponds to Lévy scaling with $\alpha \approx 0.75$ and $\gamma \approx 17$. The next challenge is to determine whether this result represents an agreement with the recorded data, and in what sense. Even more important is to what extent we can deduce new understandings both about the model construction and the observed activity from such self-consistency test.

In the study of abiotic systems, *quantitative* comparison between simulations and experiments is much coveted, although in many cases insufficient knowledge limits the comparison to be only *qualitative*. In the case of biotic systems, their autonomous

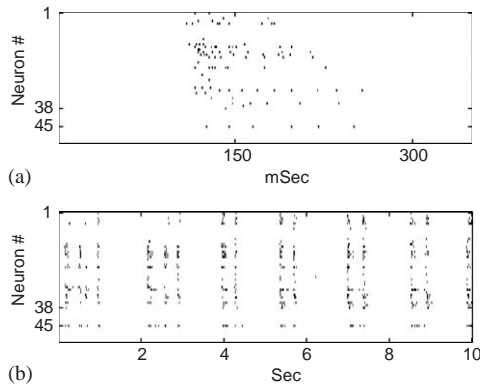


Fig. 7. Raster plot showing the response of the model neuron to the recorded network activity, as described in the text. The raster plot is shown with time resolution of 1 ms (a) and 100 ms (b).

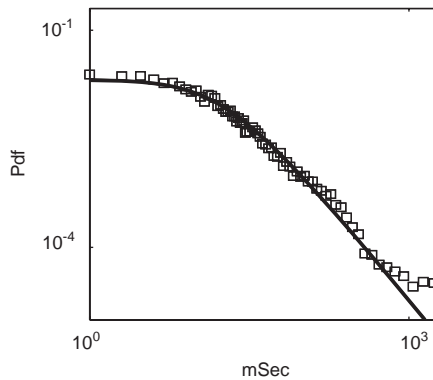


Fig. 8. The statistical scaling of the increments of the inter-spike interval time series within the SBEs. The solid line is Lévy distribution with $(\alpha = 0.75, \gamma = 25)$.

nature prevents quantitative comparison in the abiotic sense. Currently, a statistical comparison is assumed as a crucial required step towards partial quantitative comparison. The idea is to look at the averaged behavior of many systems and compare it with the averaged behavior of many simulated ones, each with a different set of parameters randomly selected from some bounded distribution. Here we adopt entirely different approach—the *generative* comparison, clarified below.

Looking at the SBEs internal structure of activity (Fig. 1), clearly each neuron in the network has its own pattern of temporal activity (time series). These individual patterns are not arbitrary, as can be discovered by evaluating the dendogrammed matrix of inter-neurons correlations [9,32]. An usual statistical comparison in this case would be first to evaluate the averaged Lévy-like distributions of the recorded neurons. Next, similar averaged distribution for modelled neurons with different parameters would be

compared with the averaged recorded one. In our generative approach, the statistically averaged activity is replaced by construction of a representative neuron of the recorded activity. An example of such construction is illustrated in Fig. 3. The latter should be compared with the model neuron behavior shown in Fig. 12.

The modelled neuron can be quantitatively compared with the “representative” recorded neuron by adjusting the model parameters. Yet, for the reasons explained, we avoid doing so. Especially since most neurons in the network show similar level of deviation from the representative one as the model neuron shows.

4. Utilizing the generic network model

With a satisfactory generic neuron model at hand, we proceed to study the behavior of generic networks composed of the M–L elements connected via the Tsodyks–Markram pre-synaptic dynamics. The network connectivity (of 20–50 elements) is taken to be all-to-all, with the synaptic strengths being drawn from normal distribution. Following physiological data [33], 80% of the neurons are selected to be excitatory ones, and the rest 20%—inhibitory ones. In Fig. 9, we show a typical realization of a selected synaptic strengths.

One of the basic puzzles related with the activity of cultured networks is about the source of self-generated activity in an isolated network that does not receive any external stimulations or chemical triggering signals. Recently, it has been proposed by Baruchi and Ben-Jacob [10] that the glia cells might participate in generation, maintenance and regulation of the cultured networks activity, utilizing external and internal (intra-cellular) biochemical messages (triggering and information-carrying signals). At this stage, as the above is yet to be converted into a modelled description, we simply represent its “maintenance role” by adding a random walk activating current. Later, we will demonstrate the ability of the network to self-regulate

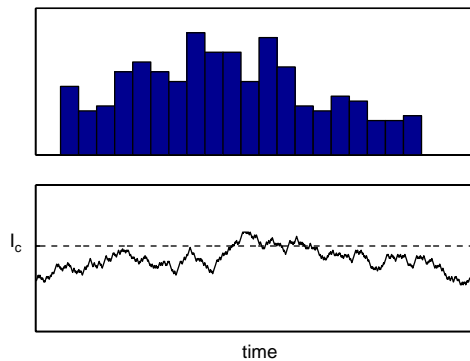


Fig. 9. Typical realization of synaptic strength and regulative “maintenance” current used in the simulations of network activity. The synaptic strengths are drawn from normal distributions, as exemplified for the case of excitatory–excitatory coupling (top). Bottom: typical realization of activating current. A firing of action potential is possible whenever a current is above the threshold value I_c .

its activity by manipulating the statistical properties of such “maintenance” current. To keep a proper balance between the above current and inputs received from other neurons via the synaptic connections, the additional current I_{ad} is limited to the range $-0.098 \mu\text{A}/\text{cm}^2 \leq I_{ad} \leq 0.002 \mu\text{A}/\text{cm}^2$. For this range, in the absence of additional input signals, each of the neurons spends most of the time within its excitable phase. So that the scaling properties of its temporal activity are mainly induced by signals received from the other neurons. We emphasize that in the model networks studied here, all the model neurons (M–L elements) have the same parameters and the variations of neuronal “self-identities” are introduced only through the distribution of the synaptic strengths. Currently, in the studies of model neural networks there is a tendency to simulate networks with as many neurons as computer power permits. The approach presented here is to simulate networks with the minimal required number of elements. The rationale for this approach is two fold. First, experimental studies of Segev et al. [6,34] demonstrated that 50 neurons networks share many generic features with larger networks. Second, simulating small networks makes it easier to identify which of the complex modes of temporal behavior are connected with special inherent neuronal features, vs. modes of complexity simply resulting from size effect of general non-linearly coupled non-linear dynamical elements. Be as it may, still a minimal number of neurons is required for them to act as a new entity. It has been shown in Ref. [25] that inclusion of inhibitory neurons imparts the networks with a more flexible mechanism for the generation of synchronized bursting events. The lowest feasible limit of inhibitory neurons to be included is 4, for the naive reasoning of keeping some meaning to the notion of variations between neurons. This, together with the physiological knowledge about the ratio between excitatory and inhibitory neurons, motivated us to simulate networks starting with only 20 neurons and up to about 50.

The above generic model networks generate SBEs with many generic features similar to the observed ones. A typical raster plot of the simulated activity is shown in Fig. 10. We turn now to discuss in more details the simulated individual neurons activities and the statistical scaling properties of the SBEs time series.

4.1. *The intra-SBEs neuronal activity*

As for the real networks, each neuron in the simulated networks has its own pattern of firing (time-series). In Fig. 11, we show the variations in the neuronal activity both between different SBEs and between different neurons. Comparing these results with the recorded ones, shown in Fig. 2, reveals that while the averaged values in both cases are similar, the real networks exhibit much larger variations. We will return to this phenomenon later on.

Next, following the analysis of the recorded network presented in Section 2, we reconstruct a representative neuron for the simulated network. The histogram of the increments in the inter-spikes intervals of a representative neuron is shown in Fig. 12. As for the representative neuron of the recorded activity, the distribution can be approximated by a symmetric Lévy distribution (the appendix). Adjustment of the model networks parameters can yield a quantitative agreement between the simulated and recorded distributions [25,35]. However, here we focus on complementary

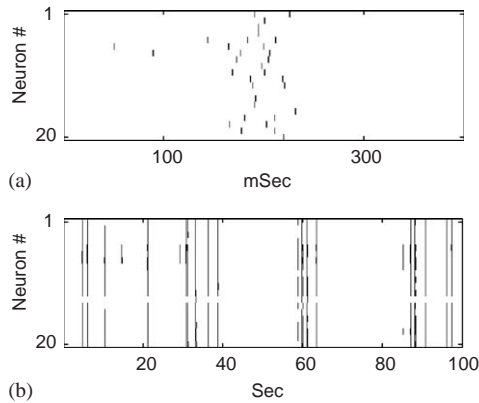


Fig. 10. Raster plot, illustrating the activity of a simulated network. The simulated network exhibits activity similar to that of cultured network. Namely, SBEs which are separated by periods of sporadic activity. The raster plot is shown in resolution of 1 ms (top), and 100 ms (bottom).

type of comparison between observations and model simulations. That is, we compare the variations in the distributions of different neurons in the recorded vs. the variations in the modelled networks [36]. Doing so, we found that the former exhibits far larger variations (details will be presented elsewhere). This is in agreement with the newly proposed realization about the ability of living systems to generate large self-regulated variations, pointed out in the introduction. The above comparison, together with the studies about the effect of synaptic strengths on the network behavior (Section 5.1), provide clues that variations between neuronal temporal activities are mainly regulated by other mechanisms than the modulation of synaptic strengths.

4.2. The statistical scaling properties of the SBEs binary sequences

The simulated SBEs binary sequences are constructed following the same “prescription” used to construct the recorded ones (Section 2). A bar-code representation of a simulated sequence is shown in Fig. 13 with the corresponding histogram of the inter-SBE intervals. It shows the same characteristic features as the recorded ones: I_{\min} , I_{mp} , I_{av} and long-tail behavior. We also show in this figure the sequence of the increments $\Delta(i)$ of the intervals, to illustrate the symmetry between the positive and negative ones, which justifies the approximation of the distribution of $\Delta(i)$ with a zero-mean symmetric Lévy distribution shown in Fig. 14. Again, a quantitative comparison between a recorded activity and a simulated one can be obtained by parameters adjustment. But, following the rationale explained earlier, we proceed to compare the pattern of the variations of the recorded activity and those of the simulated behavior, instead of “investing” in parameters adjustment. In this regard, we emphasize again that the differences in the averaged statistical parameters, say α and γ , between two cultured networks

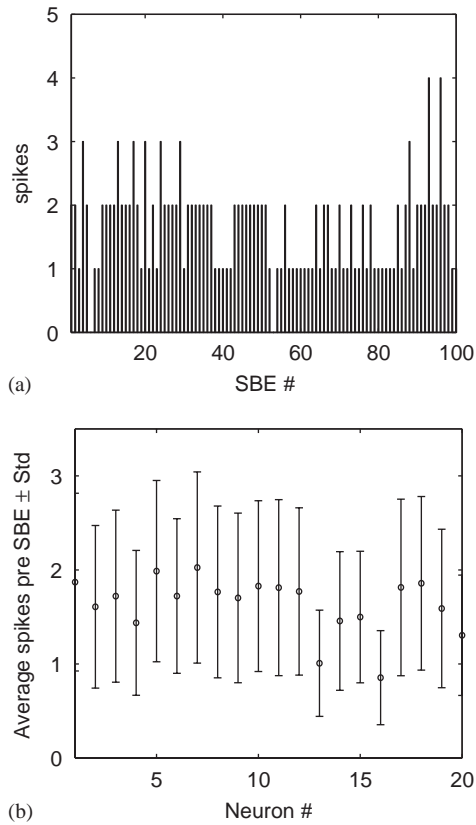


Fig. 11. Variations in the rate of firing for neurons in a simulated network: (a) Number of spikes released by individual neuron varies for different SBEs. Average spikes released by different neurons also vary (b), though the variation is smaller than the one for cultured networks (compare with Fig. 2b).

grown under the same conditions are not smaller than the differences between them and those of a simulated network. An example of a variations comparison is shown in Fig. 15, looking at the scaling of the second moment $\langle \Delta^2 \rangle$ as function of the sequence length (see the appendix for details). The scaling of $\langle \Delta^2 \rangle$ for the simulated activity is very similar to the ones obtained for artificially constructed sequence (the appendix). On the other hand, $\langle \Delta^2 \rangle$ has very different scaling behavior for the recorded sequence, thus hinting about underlying self-regulation mechanisms utilized by the cultured networks.

5. Additional clues about self-regulation deduced from model simulations

Two mechanisms which represent self-regulation were externally imposed (i.e., they do not vary according to the properties of the consequent dynamics they generate) on

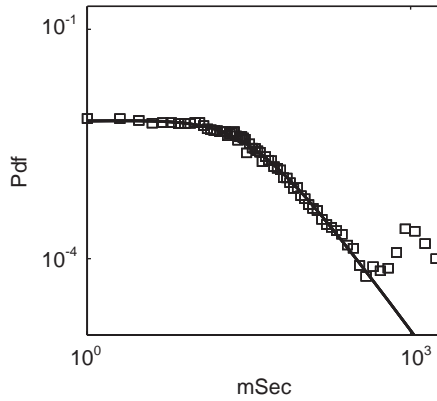


Fig. 12. Temporal statistics of the sample neuron from simulated network. All of the neurons are connected by dynamic synapses, as described in Ref. [17]. The solid line is a zero-mean symmetric Lévy distribution with ($\alpha = 0.85$, $\gamma = 40$).

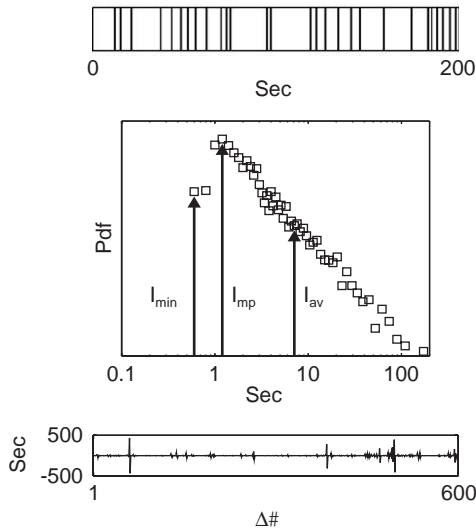


Fig. 13. Temporal activity of simulated networks. The interval series was obtained from the digitized binary sequence (top), as explained in the text. Middle: distribution of inter-event intervals possesses the same characteristic features (I_{min} , I_{mp} and I_{av}) as the cultured networks do. To illustrate the lack of directionality in the time-series, a sequence of interval increments is shown (bottom), which shows symmetry between positive and negative increments.

the model: (1) distribution of the synaptic strengths; and (2) “maintenance” current. In this section, we use the model in search for clues how these features might be utilized by cultured networks for self-regulation of their activity.

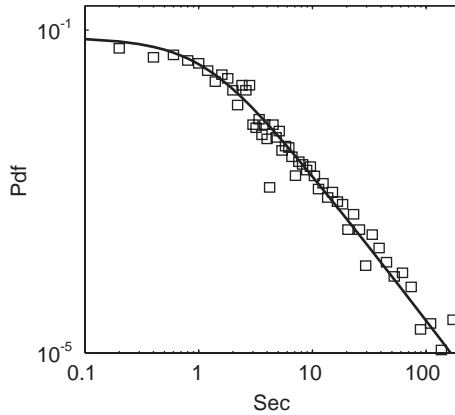


Fig. 14. Temporal statistics of the simulated network. Distribution of $\Delta(i)$. The solid line is a zero-mean symmetric Lévy distribution with $(\alpha = 0.8, \gamma = 15)$.

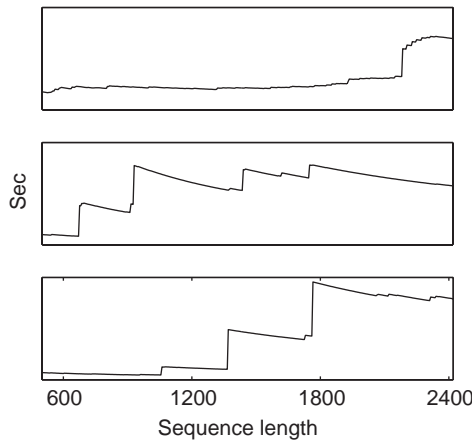


Fig. 15. Scaling of the second moment $\langle \Delta^2 \rangle$ with sequence length is shown to illustrate differences in the temporal organization of activity between real and simulated networks. Simulated network (middle) exhibits scaling of $\langle \Delta^2 \rangle$ similar to one of artificially constructed Lévy series (bottom), whilst the recorded activity of cultured networks (top) reveals different dynamics.

5.1. Possible effects of synaptic regulation

First, we check the effect of changing only the average of the synaptic strengths while preserving the shape of the distribution (the ratios between the A_{ij}). We also keep the same regulative “noise” current level and statistics. Interestingly, such changes (within limits) mainly affect the intra-SBEs neuronal activity with relatively very weak effect on the statistical properties of the SBEs times series itself. For higher A_0 , the SBEs become wider and with more intense internal neuronal activities, as shown in Fig. 16.

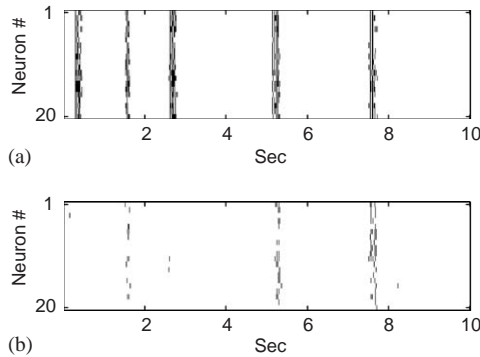


Fig. 16. The effect of synaptic strength on the pattern of correlated activity. The 10-fold increase in *all* synaptic strengths (top) leads to denser *SBEs*, as compared with the original synaptic strengths (bottom). The time bin size is 10 ms.

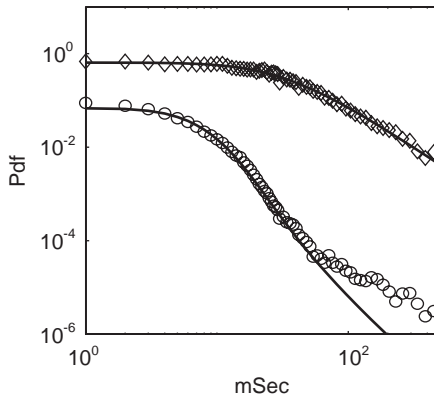


Fig. 17. The effect of synaptic strength on the distribution of $\delta(i)$. When all of the synaptic strengths are increased 10 fold (circles), the distribution parameters change as compared to those of the original synaptic strength (diamonds). Fit parameters are : ($\alpha = 0.85, \gamma = 40$) for the original synaptic strengths and ($\alpha = 1.8, \gamma = 5$) for the 10-fold increased synaptic strengths. The distributions were shifted for clarity.

At the same time, the statistical properties of the neuronal firing vary. In particular, the distribution of the increments becomes closer to a Gaussian ($\alpha = 2$), thus losing its scale-free feature (Fig. 17). With higher synaptic strengths, it is easier for the neurons to excite each other. Thus, the resulted wider and denser *SBEs*. However, as the balance between the A_{ij} is preserved, the effect on the inter *SBE* intervals distribution is much weaker, since synchronized bursting events are collective phenomena per se, involving activity of *both* excitatory and inhibitory neurons. Hence, what might affect the rate of *SBE* is a proper balance (or, more correctly, lack of balance) between excitatory and inhibitory strengths. These findings might provide an important clue with regard to the special observed behavior of some large networks, exhibiting partitioning of the *SBEs*

into sub-groups, each with its own characteristic intra-SBE neuronal activity [9]. It has been proposed that such a partitioning reflects the fact that the large networks are composed of inter-mingled smaller (within the 1mm correlation length) sub-networks. And therefore the combined network can generate different kinds of SBEs, each with its own internal pattern of neuronal activity. It has been further proposed that each kind of SBE is generated by a different sub-network of neuronal connectivities being dominant. Our findings about the effect of A_0 imply that in principle it is possible to have two mingled sub-networks each with a different synaptic strength, so that they will mutually generate two kinds of SBEs. In Fig. 18, we show a preliminary “feasibility” test of this idea. To test for the existence of different kind of SBEs, we have used the method of dendrogrammed cross-correlation matrix between the generated SBEs, as described in Refs. [9,32]. As is demonstrated for un-partitioned network, only single kind of SBEs is generated. On the other hand, when the network is partitioned into mingled sub-networks, different kinds of SBEs can be mutually generated. In the shown “feasibility” test, a 40 neurons network is partitioned into two 20 neurons networks, one with three times larger A_0 than the other. The two sub-networks are mingled via six joint neurons. While only preliminary, this result illustrates the possible important role of synaptic regulation (more details will be presented elsewhere).

5.2. Possible role of the regulative “noise” current

The phase-space analysis implies that the characteristic inter-SBE interval length is mainly determined by the neurons’ dwell time within the excitable phase. Therefore, it is expected that the statistical properties of the triggering current can have strong effect on the inter-SBE interval distribution.

To test the effects of the excess current statistics, we increased 100 fold the absolute value of a current step, together with a 100-fold increase in the update time (the current time steps), thus producing a new signal with larger correlations. This extra-structure forces the index of stability to decrease ($\alpha = 0.58$) and causes prominent change in the dispersion parameter ($\gamma = 90$). Hence, by imposing a temporal structure upon the regulative “noise” current, it is possible to regulate statistical properties of the network activity.

In addition, we found that reducing the time correlations in the noise current leads to a nearly Gaussian distribution in the increments of the SBEs intervals. These observations imply that by self-regulation of the noise current, for example by glia cells or by specific special neurons, the network can regulate the statistical properties of the SBEs activity.

As a “feasibility” test of the above idea, we have replaced the artificially produced current with a “regulating” current constructed from the recorded neurons. We mentioned earlier that some neurons fire at much higher rate (10 fold and more) than the averaged neuronal firing rate and have different statistical scaling properties than the other neurons. Guided by the idea that such neurons might serve to maintain the spontaneous activity, we have selected two of them. One to be an excitatory and the other an inhibitory. The regulating current fed into all the neurons in the model network was composed of both of them (with a 2.5 s lag time), *in addition to the currents*

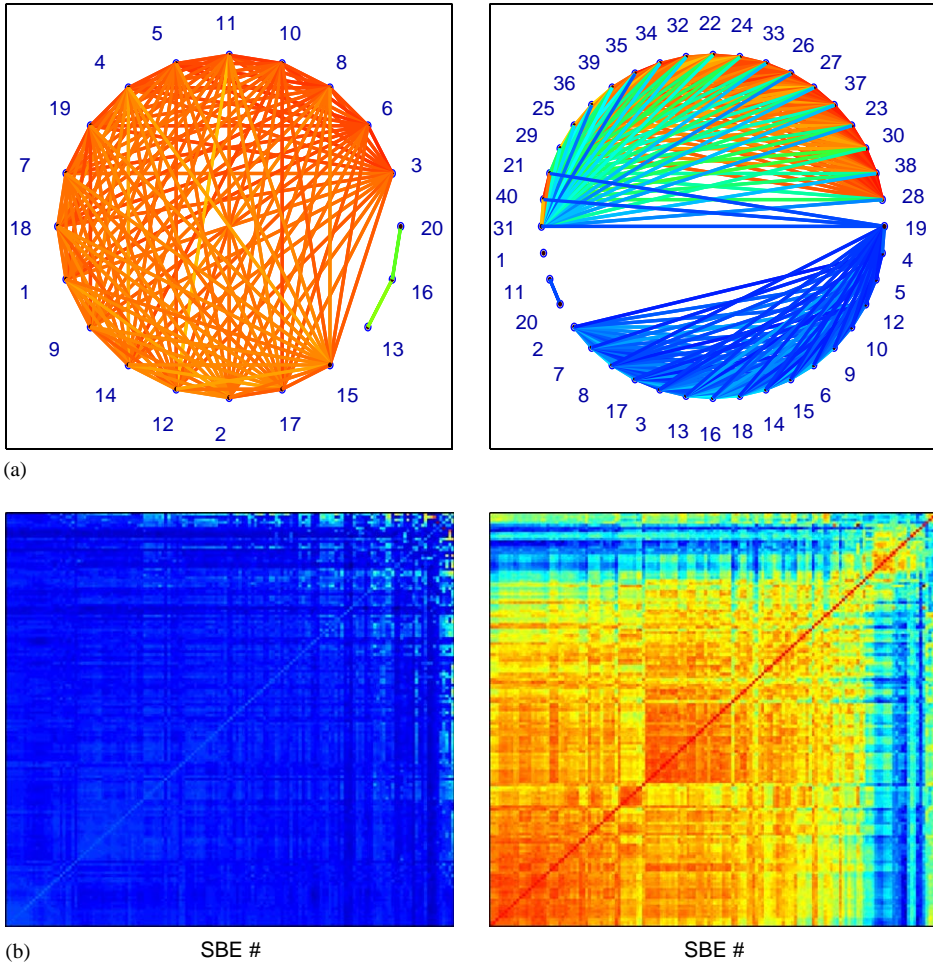


Fig. 18. Testing the effect of “engineered” synaptic connections using the dendrogrammed matrix method, as described in references [9,32]. Top: left: correlation circle for network with normal distribution of synaptic strengths (the network has 20 neurons, the inhibitory ones being nos. 13,16 and 20); right: correlation circle for two networks, of 20 neurons each. For two networks, synaptic strengths are normally distributed. For the second network (cells 21–40), the strengths are three-fold larger. In addition, there are cross-synaptic connections between two networks, limited to neurons 10–30. Bottom: the corresponding dendrogrammed correlation matrices of the SBEs.

they receive through the model network synaptic connections between the neurons. The results of this second feasibility test are shown in Fig. 19. The statistical scaling (Lévy) parameters become much closer to the observed ones. We reflect on the possible implications of these results in the next section.

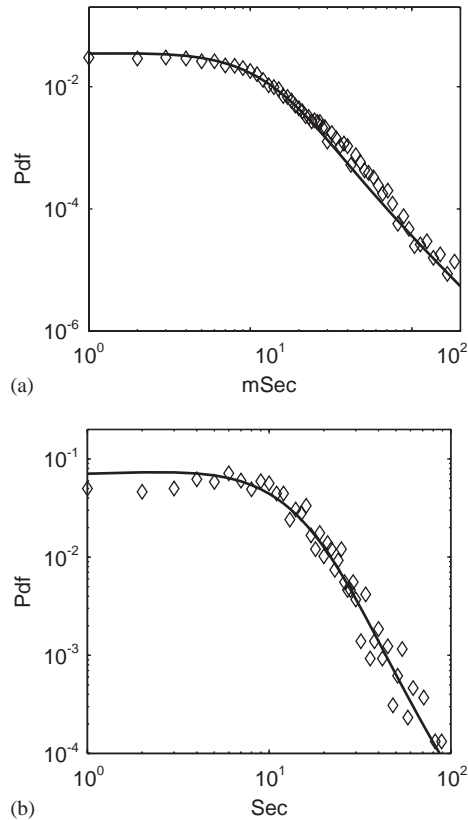


Fig. 19. The characteristics of temporal activity obtained when artificially produced “maintenance” current has been replaced with a “regulating” current, constructed as is explained in the text. (a) Distribution of the increments of the inter-spike intervals. (b) Distribution of $\Delta(i)$. The solid lines are zero-mean symmetric Lévy distributions with $(\alpha = 1.6, \gamma = 7.5)$ and $(\alpha = 1.72, \gamma = 8.5)$, respectively.

6. Concluding remarks

Thus far, we have included the minimal requirements that a model network must fulfill in order to reproduce the observed statistical scaling behavior. We have also been able to deduce new hints and clues about self-regulation motives in cultured network, utilizing generative comparison between simulations and observations. For reasons described earlier, we have studied small-scale model networks, comprising only 20–50 cells. A very interesting issue concerns the connection between networks size and its pattern of activity, since experimental observations show that networks of different sizes share the same generic features. Namely, all of the networks exhibit synchronized modes of activity and Lévy-like temporal scaling in the appropriately chosen observable. These features hint on possible common regulation pathways that might be utilized by neuronal networks of different sizes.

As the number of neurons in the network grows, so does also the number of potential SBE triggers. Hence, a large network is expected to generate SBEs at a higher rate, unless some regulating mechanism is acting. Two such mechanisms have been considered in this paper : (1) regulation of synaptic strengths, by which it is possible to control temporal activity of neurons within the SBEs, and (2) structured maintenance current, which shapes the temporal ordering of the SBEs.

We have shown that imposing an architecture on the strength of coupling between the cells can have a profound effect on statistical properties of neuronal temporal activity. This is in accord with current belief that synaptic plasticity (i.e., modulation of synaptic strength) shapes the information processing and response properties of neuronal network. Thus, an additional information about dynamics of networks may be deduced by considering the long-term effects (taking place on the scale of minutes and hours). For instance, these effects can explain the observed long-term correlation in the time series of SBEs. On these large time scales, the detailed behavior of neurons is less important. Indeed, it is shown in Ref. [25] that certain features relating to the long-term dynamics can be reproduced using simple Integrate-and-Fire description of individual neurons.

Our observations that the scaling properties of networks' activity may be modulated by structured "maintenance" current immediately bring to mind the possibility of mutual regulation. Namely, that the activity of small densely connected assembly is regulated by the other regions of network. If true, this hypothesis might reflect the complex self-regulated hierarchical organization of neuronal networks, which is currently believed to be a key factor responsible for networks' unique flexibility and adaptability. The feasibility test, whereby a model network has been fed with regulating current composed of two fast spiking neurons, has been a first step towards this direction. Our assumptions are further strengthened by results of recent research, where it is shown that cultured neuronal networks normally self-organize into small, compact clusters connected by bundles of axons [24].

One of the intriguing puzzles relates to the origin of spontaneous activity in cultured neuronal networks. In our studies, this problem has been resolved by providing each cell with an artificial structured maintenance current. Recent evidence [15] indicates that neurons get and respond to signals from their surrounding glial cells, thus making the glia-produced signals possible biological correlate of our structured maintenance current. Largely speaking, astro-glia regulate the synaptic dynamics, and micro-glia regulate the dynamics of somata [15]. More specifically, the astro-glial regulatory mechanisms can correlate the temporal activity of a given synapse with the synaptic strength of other synapses, either on the same neuron or on different neurons. These mechanisms have characteristic time scales ($>$ seconds) comparable to those of the inter-SBEs temporal ordering, and characteristic length scales between the soma $\approx 10 \mu\text{m}$ and the $\approx 1000 \mu\text{m}$ spikes correlation length (i.e., the action potentials propagation length during the $\approx 1 \text{ ms}$ time width). These features imply that, from pattern formation perspective, the observed spontaneous neuronal activity represents only part of the cultured networks dynamical behavior. The complementary parts of the dynamics are the formation of intracellular calcium waves, inter-cellular direct chemical signaling mechanisms and extra-cellular chemical communication. Thus, the next stage in

modelling of cultured networks activity calls for integration of a model of the kind presented here with underlying fabric of glia cells acting as an excitable media.

Acknowledgements

We are very thankful to Ronen Segev and Netta Cohen for collaboration at the early stage of the studies presented here. We have benefited from illuminating conversations with David Horn, Itamar Procaccia and Herbert Levine. This research was supported in part by a grant from the ISF, the Samuelli Institute, and the Maguy-Glass chair in Physics of Complex Systems.

Appendix A. A concise description of Lévy distributions

For simplicity, we present here the Lévy distributions with regard to the specific examples of the increments $\Delta(i)$ of the intervals between “1”s for a general binary sequence. The general Lévy distribution $L(\Delta)$ is characterized by the following four parameters: α , γ , δ and β [11–13]. The increments in the intervals between the SBEs were approximated with the zero-mean symmetric Lévy distribution for which $\delta = 0$ and $\beta = 0$. This distribution is given by

$$P_{\alpha\gamma}(\Delta) = \frac{1}{\pi} \int_0^\infty \exp(-\gamma q^\alpha) \cos(q\Delta) dq . \tag{A.1}$$

A typical example of a symmetric Lévy distribution on a log–log scale is shown in Fig. 20. As is illustrated, the slope of the long tail (scale-free part of the distribution) is controlled by α (the index of stability, or the tail parameter), and its slope is equal to $-(\alpha + 1)$. The second parameter γ is the dispersion factor that sets the location of

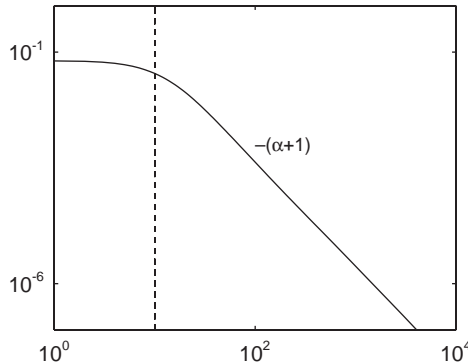


Fig. 20. A typical realization of Lévy distribution is shown on double logarithmic scale to illustrate the intuitive meaning of α and γ parameters. The index of stability, α , defines the slope of long-tail decay of a distribution, while γ sets a location of the bending point.

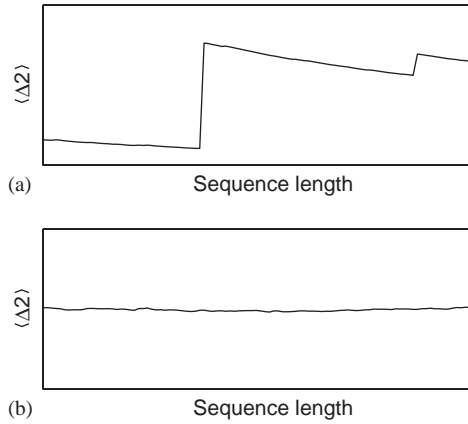


Fig. 21. Scaling of the second moment, $\langle \Delta^2 \rangle$, is shown to illustrate divergence of sequence variance. For $\alpha = 2$, $\langle \Delta^2 \rangle$ converges to the variance of the sequence, σ^2 (bottom). On the other hand, $\langle \Delta^2 \rangle \rightarrow \infty$ for $\alpha < 2$, as illustrated on the upper panel.

bending. Two special cases of the zero-mean symmetric Lévy distribution are: (1) the Cauchy case with $(\alpha = 1, \beta = 0)$, in which

$$P_{\alpha=1, \gamma}(x) = \frac{\gamma}{\pi(\gamma^2 + x^2)} ; \tag{A.2}$$

(2) The Gaussian limit for $\alpha \rightarrow 2$ in which

$$P(x) = \frac{1}{\sqrt{2\pi}\sigma} \exp\left(-\frac{x^2}{2\sigma^2}\right) , \tag{A.3}$$

where the standard deviation is given by $\sigma = \sqrt{\gamma}$. Note that $\alpha = 2$ is a singular limit of Eq. (A.1), hence it is not simply derived by inserting $\alpha = 2$ in this equation. It reflects the fact that while for $\alpha = 2$ the second moment of the distribution is bounded, for any $\alpha < 2$ the second moment is unbounded for infinite sequence. In Fig. 21, we show the scaling of $\langle \Delta^2 \rangle$ as function of the sequence length for two constructed realizations of Lévy distributions for different sets of the (α, γ) parameters.

Next, we briefly discuss the additional Lévy parameters δ and β . A shifted finite-mean symmetric Lévy distribution is centered at δ (Fig. 22a), which is defined as the maximum of the distribution or the most probable increment $X_{mp} = \delta$. For symmetric distributions, the average value is equal to the most probable one, i.e., $X_{av} = X_{mp}$. The fourth parameter, β , is connected with asymmetry about δ (Fig. 22b). It is reflected in the differences between the average values of the variables and their most probable values. For a distribution of increments with $\delta = 0$, the deviation of β from zero indicates that the sequence represents an underlying time-directionality in the process that generates it. Generally speaking, if the average interval between SBEs does not change but $\beta \neq 0$, it hints about regulation of time directionality.

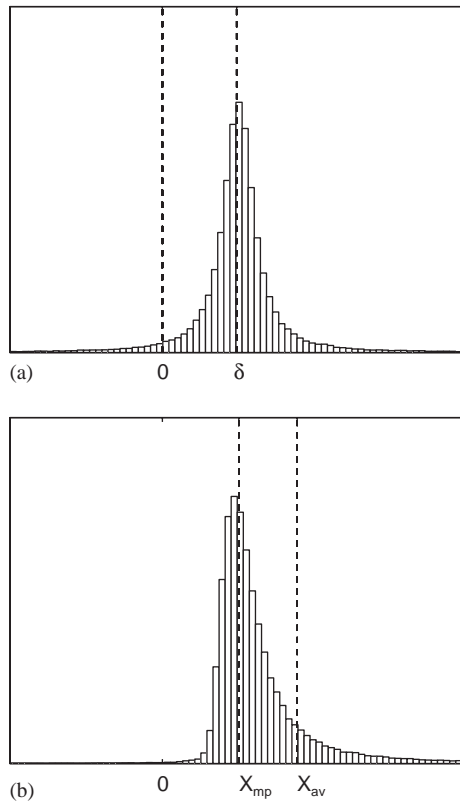


Fig. 22. The β and δ parameters of the Lévy distribution reflect its symmetry properties. For symmetric distributions (a), $\beta = 0$ and δ is identical to the average value of X . When a distribution is skewed ($\beta \neq 0$) δ is a most probable value of X , as (b) exemplifies.

References

- [1] E. Ben-Jacob, Bacterial self-organization: co-enhancement of complexification and adaptability in a dynamic environment, *Philos. Trans. R. Soc. London A* 361 (2003) 1283–1312.
- [2] E. Ben-Jacob, When order comes naturally, *Nature* 415 (2002) 370.
- [3] E. Ben-Jacob, I. Cohen, H. Levine, Cooperative self-organization of microorganisms, *Adv. Phys.* 49 (4) (2001) 395–554.
- [4] H. Levine, E. Ben-Jacob, Biological pattern formation: examples, issues and strategies, *J. Phys. Biol.*, in press.
- [5] J. Horgan, From complexity to perplexity, *Sci. Am.* 95 (1995) 74–79.
- [6] R. Segev, M. Benveniste, Y. Shapira, E. Hulata, N. Cohen, E. Kapon, E. Ben-Jacob, Long term behavior of lithographically prepared in vitro neural networks, *Phys. Rev. Lett.* 88 (2002) 118 102.
- [7] R. Segev, Y. Shapira, M. Benveniste, E. Ben-Jacob, Observations and modeling of synchronized bursting in 2d neural networks, *Phy. Rev. E* 64 (2001) 011920.
- [8] R. Segev, E. Ben-Jacob, Spontaneous synchronized bursting in 2d neural networks, *Physica A* 302 (2001) 64–69.

- [9] R. Segev, I. Baruchi, E. Hulata, E. Ben-Jacob, Hidden neuronal correlations in cultured networks, *Phys. Rev. Lett.*, in press.
- [10] I. Baruchi, E. Ben-Jacob, Self-regulated formation of connectivity networks in the hidden space of neuronal correlations. *NeuroInformatics* (in process), 2003.
- [11] W. Feller, *An Introduction to Probability Theory and its Applications*, Wiley, New York, 1968.
- [12] J. Bertoin, *Lévy Processes*, Cambridge University Press, Cambridge, 1996.
- [13] R.N. Mantegna, H.E. Stanley, *An Introduction to Econophysics*, Cambridge University Press, Cambridge, 2000.
- [14] B. Mandelbrot, The variation of certain speculative prices, *J. Bus.* 37 (1963) 392–417.
- [15] P.R. Laming, et al., Neuronal-glia interactions and behavior, *Neurosci. Biobehav. Rev.* 24 (2000) 295–340.
- [16] E. Hulata, I. Baruchi, R. Segev, Y. Shapira, E. Ben-Jacob, Self-regulated complexity in cultured neural networks, *Phys. Rev. Lett.*, submitted for publication.
- [17] M. Tsodyks, A. Uziel, H. Markram, Synchrony generation in recurrent networks with frequency-dependent synapses, *J. Neurosci.* 20 (2000) RC50(1–5).
- [18] A.L. Hodgkin, A.F. Huxley, A quantitative description of membrane current and its application to conduction and excitation in nerve, *J. Physiol.* 117 (1952) 500–544.
- [19] C. Koch, *Biophysics of Computation*, Oxford University Press, New York, 1999.
- [20] R. FitzHugh, Impulses and physiological states in theoretical models of nerve membrane, *Biophys. J.* 1 (1961) 445–466.
- [21] J.S. Nagumo, et al., An active pulse transmission line simulating nerve axon, *Proc. IRE* 50 (1962) 2061–2070.
- [22] C. Morris, H. Lecar, Voltage oscillations in the barnacle giant muscle fiber, *Biophys. J.* 35 (1981) 193–213.
- [23] L.F. Abbott, T. Kepler, *Model Neurons: From Hodgkin–Huxley to Hopfield*, *Statistical Mechanics of Neural Networks*, Springer, Berlin, 1990.
- [24] R. Segev, M. Benveniste, Y. Shapira, E. Ben-Jacob, Formation of electrically active clustered neural networks, *Phys. Rev. Lett.* 90 (16) (2003) 168101.
- [25] E. Persi, D. Horn, V. Volman, E. Ben-Jacob, Modeling of synchronized bursting events: the importance of inhomogeneity, *Neural Comput.*, submitted for publication.
- [26] J. Rinzel, G.B. Ermentrout, *Models of Neural Excitability*, MIT Press, Cambridge, MA, 1989.
- [27] B. Gutkin, G.B. Ermentrout, Dynamics of membrane excitability determines interspike interval variability: a link between spike generation mechanisms and cortical spike train statistics, *Neural Comput.* 10 (1998) 1047–1065.
- [28] N. Cohen, The development of spontaneous beating activity in cultured heart cells: from cells to networks, Ph.D. dissertation, Technion (2001).
- [29] N. Cohen, H.G. Rotstein, E. Braun, Self-organized dynamics of cultured heart cells, in preparation.
- [30] R.S. Zucker, Short-term synaptic plasticity, *Ann. Rev. Neurosci.* 12 (1989) 13.
- [31] L.F. Abbott, S.B. Nelson, Synaptic plasticity : taming the beast, *Nat. Neurosci.* 3 (2000) 1178–1183.
- [32] I. Baruchi, Formation of hidden spatio-temporal correlations observed in the lithographically prepared neuronal networks, M.Sc. Thesis, Tel-Aviv University, June 2003.
- [33] M. Abeles, *Corticonics*, Cambridge University Press, Cambridge, 1991.
- [34] R. Segev, Self-organization of in-vitro neuronal networks, Ph.D. Dissertation, Tel-Aviv University, 2002.
- [35] M. Marinaro, S. Scarpetta, Modeling of spontaneous synchronized periodic activity observed in in-vitro networks, *Neurocomputing* 52 (2003) 89–95.
- [36] N. Raichman, personal communication.